Desalination and Water Treatment 317 (2024) 100207

Contents lists available at ScienceDirect

Desalination and Water Treatment

journal homepage: www.sciencedirect.com/journal/desalination-and-water-treatment/

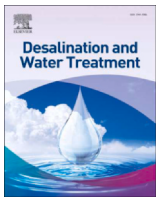

Adsorption–desorption behavior of halloysite clay for Cu^{2+} ions and recovery of copper by electrodeposition method

Le Thi Duyen[a,c,*], Bui Hoang Bac[b,c,d]

[a] Department of Chemistry, Faculty of Basic Science, Hanoi University of Mining and Geology, Viet Nam
[b] Faculty of Geosciences and Geology Engineering, Hanoi University of Mining and Geology, Viet Nam
[c] HiTech-CEAE Research Team, Hanoi University of Mining and Geology, Viet Nam
[d] Innovations for Sustainable and Responsible Mining (ISRM) Research Group, Hanoi University of Mining and Geology, Hanoi, Viet Nam

ARTICLE INFO

Keywords:
Halloysite
Cu^{2+} adsorption
Cu^{2+} desorption
Recovery of Cu
Electrodeposition

ABSTRACT

Halloysite sample, obtained from Phu Tho province, Vietnam, was utilized to investigate the adsorption behavior of Cu^{2+} ions. Several factors influencing Cu^{2+} adsorption efficiency and capacity were explored, including pH value, contact time, adsorbent dose, and initial Cu^{2+} concentration. Under optimal conditions (0.8 g of halloysite per 50 mL of solution, an initial Cu^{2+} concentration of 40 mg/L, pH 6.2, a contact time of 80 min, and a temperature of 25 °C), the study yielded an adsorption efficiency of 85.19% and a capacity of 2.14 mg/g for Cu^{2+} ions. Adsorption isotherm analysis was conducted using the Langmuir and Freundlich models, while the kinetics of the adsorption process were investigated through the first-order pseudo and second-order pseudo models. Furthermore, the desorption of Cu^{2+} ions and the recovery of Cu metal were explored, with a recovery efficiency of Cu reaching 94.65% under suitable conditions (0.3 g mass of halloysite, a current of 7.5 mA, and an electrolytic time of 5 h at 60 °C). These findings suggest the potential application of halloysite clay for removing Cu^{2+} ions from polluted water, recovering Cu metal, and reusing the adsorbent.

1. Introduction

Presently, the world is confronted not only with a water scarcity crisis but also with significant water quality concerns. Factors like population growth, urban and industrial expansion, and increased agricultural activities are the primary contributors to water pollution, which has adverse impacts on water quality and human health. Consequently, water quality issues have gained considerable attention from both the public and the scientific community. Numerous studies have proposed various methods for treating heavy metals in water, including chemical precipitation, electrochemical precipitation, membrane separation, ion exchange, adsorption, biological methods, and more. Among these methods, adsorption has garnered substantial research interest in recent years. Natural adsorption materials such as red mud [1], zeolite [2], bentonite [3], kaolinite [4], apatite [5–7], halloysite [8–10], as well as natural polymers like chitin, chitosan [11], recycled materials from agricultural byproducts [12–14] and recently mesoporous materials produced from waste biomass materials [15,16] have attracted widespread attention from scientists worldwide. These materials offer advantages such as low cost, high adsorption efficiency, and environmental friendliness, especially for wastewater treatment applications.

In recent years, halloysite, a natural mineral belonging to the kaolin group, has gained significant attention from scientists, and has found numerous applications due to its exceptional characteristics. These characteristics include its ultra-small tube-like structure, non-toxicity, high mechanical strength, and cost-effectiveness compared to materials like nanotubes. Consequently, halloysite has undergone extensive research and has been applied in various fields, including pharmaceuticals [17,18] medicine [18,19], catalysis, high-end materials, agriculture [18], and environmental [19–24] applications.

Copper (Cu) is an essential trace element in the human body, but when its concentration exceeds allowable limits, it can become toxic. Excess copper can lead to serious health conditions, including adrenal gland insufficiency, kidney and liver damage, joint inflammation, mental disorders, osteoporosis, and even cancer. Furthermore, it is toxic to aquatic organisms at very low concentrations in water. Consequently, the removal of copper from contaminated water sources is of paramount importance. Commonly used methods for copper removal include activated carbon, clay minerals, zeolites, chitosan,

* Corresponding author at: Department of Chemistry, Faculty of Basic Science, Hanoi University of Mining and Geology, Viet Nam.
E-mail address: lethiduyen@humg.edu.vn (L.T. Duyen).

https://doi.org/10.1016/j.dwt.2024.100207
Received 4 January 2024; Received in revised form 4 January 2024; Accepted 30 January 2024
1944-3986/© 2024 The Author(s). Published by Elsevier Inc. This is an open access article under the CC BY-NC license (http://creativecommons.org/licenses/by-nc/4.0/).

apatite, biological adsorbents, and agricultural byproducts [11,24–27]. On the other hand, copper is a metal with numerous applications in daily life. Therefore, researching efficient adsorption and recovery methods for copper is also essential to prevent secondary pollution and to harness valuable metals from waste, thereby enhancing economic efficiency. The quest for effective methods to absorb heavy metals, recover them, and minimize adverse environmental impacts while regenerating the adsorbent material represents a contemporary trend. To desorb heavy metals from adsorbent materials, commonly used desorbing agents include HCl, HNO_3, NaOH, $Ca(NO_3)_2$, EDTA, etc. However, there has been no research reported on the ability to desorb and recover heavy metals without the separate steps.

Paulina Maziarza and her co-authors developed high-affinity nanocomposite materials of halloysite-Fe0 with enhanced adsorption capabilities for Pb(II)/Cd(II). However, the selectivity for As(V) and Cr(VI) was not as clear. Their adsorption-desorption studies demonstrated that the material obtained after regeneration remained effective when treated with NaBH4, allowing for the reuse of the material for high metal removal [22]. Jamileh Zare Pirhaji's research team utilized halloysite/graphene materials for the adsorption and removal of Pb(II) from water, achieving a high adsorption capacity of 42.02 mg/g. The adsorbent material could be easily regenerated using a magnet [23]. Katsuhiko ITAMI and others studied the adsorption and desorption properties of cadmium (Cd) and copper (Cu) in five types of clay minerals (montmorillonite, sericite, kaolinite, halloysite, and allophane) as representatives of commonly distributed minerals in soil environments. Desorption experiments were conducted at different pH levels, revealing that Cu had lower desorption efficiency than Cd in a $Ca(NO_3)_2$ extraction solvent [26]. S. Lukman and his research team studied the adsorption and desorption of five heavy metals: Cu, Pb, Zn, Cd, and Cr under the influence of initial pH in both single and multi-metal systems. The results showed that pH greatly influenced the adsorption/desorption of heavy metals on natural clay minerals. The selective adsorption sequence was as follows: Cr > Pb > Cu > Cd > Zn and Cr > Cu > Pb > Cd > Zn, respectively, in single and multi-metal systems. In contrast, the desorption sequence in the presence of multi-metal ions was Cr < Cd < Cu < Pb < Zn [27].

Overall, while research on heavy metal adsorption from the environment, particularly industrial wastewater, has been meticulous, studies on the desorption and recovery of heavy metals, as well as the regeneration of adsorbent materials for subsequent adsorption processes, have received less attention. Some research has been published on the desorption of heavy metals from various materials, including hydroxyapatite [28–30], montmorillonite [31], kaolinite [4], vermiculite [32], clay minerals [26], biological adsorbents [33], activated carbon, and more [34–39]. However, there are very few studies published on the desorption and recovery of heavy metals from halloysite adsorbent materials [22,23,26] and their subsequent reuse. In this paper, halloysite in the Phu Tho area, Vietnam is used to adsorb Cu^{2+} ions in a water solution. Then, they are desorbed, and Cu metal is recovered from the loaded HAL material by electrochemical precipitation in choline chloride-urea (reline) ionic liquid. This study's main advantage is that the desorption and recovery process simultaneously in an electrochemical cell with an ionic liquid medium, which represents an environmentally friendly electrochemical electrolyte. Under the effect of electric current, the desorption process is more advantageous. This method not only shortens desorption time and steps but also preserves the adsorbent material after desorption, facilitating efficient material regeneration.

2. Experiment and analytical methods

2.1. Material

The halloysite (HAL) sample used for this research was collected from the kaolin mine in Phu Tho, Vietnam. After collection, the sample was dried at 60 °C. The sample appears as a light-yellow powder (Fig. 1a). A Transmission Electron Microscopy (TEM) image reveals that the minerals in the sample possess a nano-tubular structure, a characteristic feature of halloysite minerals (Fig. 1b). Additionally, the specific surface area of the sample was measured to be 20.015 m^2/g.

The pH_{PZC} (Point of Zero Charge) value of the halloysite sample was determined using the pH drift method. In this method, 0.25 g of halloysite material was added to a 50 mL solution of 0.01 M KCl with varying initial pH values (pH_0), which were adjusted using 0.01 M HCl or 0.01 M NaOH solutions. The mixture was then vigorously stirred at 800 revolutions per minute for 30 min using a stirrer. Afterward, the solution was filtered, and the pH (pH_s) of the filtrate was measured to calculate ΔpH (1). A graph was constructed to illustrate the variation of ΔpH with pH_0. The pH_{PZC} value was identified as the pH_0 at which ΔpH = 0 [40]. The results indicate that ΔpH = 0 occurs at a pH_0 value of 5.99 (Fig. 2). This confirms that the pH_{PZC} of the halloysite particles is 5.99.

$$\Delta pH = pH_0 - pH_s \quad (1)$$

2.2. Adsorption of Cu^{2+} using halloysite powder

The factors influencing the adsorption of Cu^{2+} by halloysite were investigated by introducing a specific amount of halloysite material into a container containing 50 mL of a Cu^{2+} ion solution under various experimental conditions. The parameters studied included adsorption time (ranging from 10 to 120 min), solution pH (investigated from 3.07 to 6.73), the mass of halloysite powder (varied from 0.3 to 1 g), and the initial concentration of the solution (ranging from 10 to 80 mg/L). The mixture was agitated at a speed of 800 revolutions per minute using a stirrer. Following adsorption, solid-liquid separation was performed, and the liquid portion was used to quantify the remaining Cu^{2+} ions. Halloysite powder that has adsorbed Cu^{2+} ions is denoted as Cu-HAL.

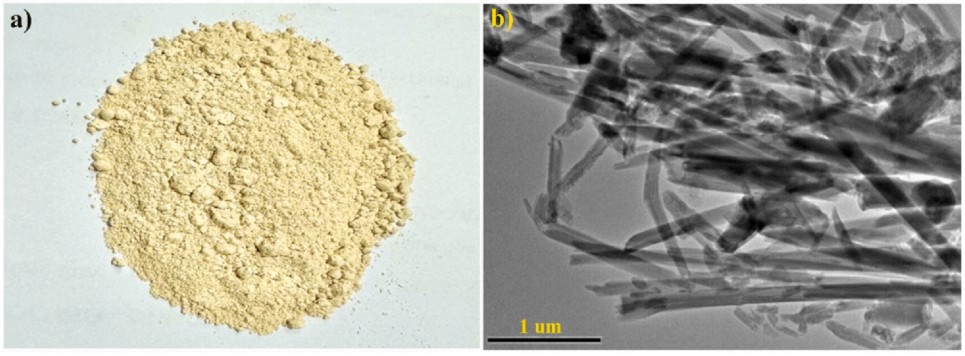

Fig. 1. HAL powder (a) and TEM image (b) of HAL.

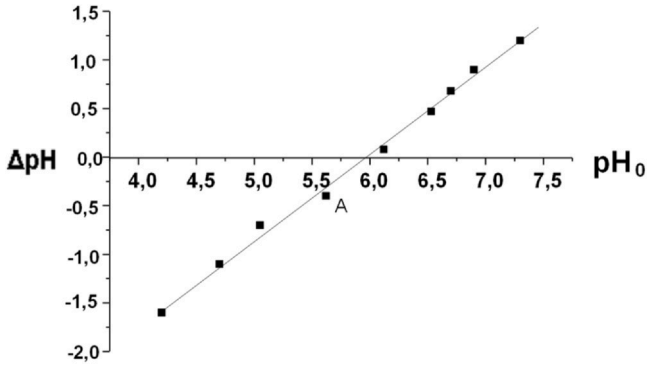

Fig. 2. ΔpH change according to pH_0 of halloysite powder.

The adsorption capacity (Q) and adsorption efficiency (H) were determined using Eqs. (2) and (3) [25]:

$$Q = (C_0 - C) \times V / m \quad (2)$$

$$H = ((C_0 - C) / C_0) \times 100 \quad (3)$$

Where: Q (mg/g) and H (%) represent the adsorption capacity and adsorption efficiency, respectively. C_0 (mg/L) denotes the initial concentration of Cu^{2+} ions. C (mg/L) signifies the concentration of Cu^{2+} ions remaining after adsorption. V corresponds to the volume of the adsorption solution (in liters). m represents the mass of the halloysite powder (in grams).

2.3. Adsorption isotherms

The Cu^{2+} adsorption capacity of halloysite is calculated using the Langmuir and Freundlich adsorption isotherms, as detailed in the following equations [25].

Langmuir linear equation:

$$\frac{C_e}{Q} = \frac{C_e}{Q_m} + \frac{1}{K_L . Q_m} \quad (4)$$

Freundlich linear equation:

$$LnQ = LnK_F + \frac{1}{n} . LnC_e \quad (5)$$

Here are the definitions of the variables involved: C_e (mg/L) represents the equilibrium concentration of Cu^{2+}. Q (mg/g) represents the equilibrium adsorption capacity. Q_m (mg/g) represents the maximum adsorption capacity. K_L is the Langmuir constant. K_F and n are the Freundlich constants.

2.4. Adsorption kinetics

The kinetics of the adsorption process are investigated using two kinetic models: the pseudo-first-order model (6) and the pseudo-second-order model (7) [25].

$$\text{Pseudo-first-order model: } \ln(Q_e - Q_t) = \ln Q_e - k_1 t \quad (6)$$

$$\text{Pseudo-second-order model: } t/Q_t = t/Q_e + 1/(k_2 \cdot Q_e^2) \quad (7)$$

In these equations: Q_e represents the equilibrium adsorption capacity (mg/g). Q_t represents the adsorption capacity at time t (mg/g). k_1 and k_2 are the rate constants for the pseudo-first-order (1/min) and pseudo-second-order (g/mg/min) kinetics, respectively.

2.5. Desorption of Cu^{2+} ions and recovery of metallic Cu by electrochemical precipitation method

2.5.1. Preparation of reline solvent

The deep eutectic solvent (DES) of reline was obtained by mixing choline chloride (ChCl) and urea (U). Choline chloride and urea were mixed in a 1:2 molar ratio in a closed container under constant stirring for 3 h at 60 °C until a homogeneous colourless liquid was formed [41].

2.5.2. The cyclic voltammetry of Cu^{2+} and Cu-HAL in the reline medium

The Cyclic Voltammetry method (CV) involves applying a specific voltage to the research electrode and, after that scanning in either the anodic or cathodic direction while observing the corresponding current. For accurate measurements, the electrode surface must be restored before measurement, the solution should not be stirred or agitated, and mass transfer occurs solely through diffusion.

The CV measurement setup typically comprises three electrodes submerged in an electrolytic solution: the Working Electrode (WE), the Reference Electrode (RE), and the Counter Electrode (CE). .

2.5.3. Desorption of Cu^{2+} and precipitation of metallic Cu onto the Au electrode surface

The process of desorbing Cu^{2+} ions from Cu-HAL and precipitating copper metal involves an electrochemical cell equipped with three electrodes:

1. The working electrode (WE) is a gold plate with a geometric surface area of 1 cm^2.
2. The reference electrode (RE) consists of a silver/silver chloride electrode immersed in a chloride solution ($Ag|AgCl|Cl^-$).
3. The counter electrode (CE) is a large-area platinum grid.

Copper recovery occurs through an electrochemical precipitation method in a reline solvent with a precipitation potential of ≤ -0.6 V and a temperature of 60 °C. Before the electrochemical process, the reline DES is purged with nitrogen gas for a minimum of 20 min and is maintained under a nitrogen atmosphere throughout the electrolysis process.

The study involves various applying current intensities: 0.5, 1, 2, 3, 5, 7.5, and 10 mA, varying the mass of the loaded HAL material (Cu-HAL) from 0.3 to 1.0 g, and studying the electrolysis time within the range of 1 to 10 h. After electrolysis, the Cu-HAL powder is filtered from the mixture, and subjected to cleaning and drying processes, and the remaining amount of copper in the powder is determined by the ICP-MS method. This analysis allows for the calculation of the recovery efficiency of copper.

3. Results and discussion

3.1. Effects of factors on Cu^{2+} adsorption efficiency and capacity of halloysite

3.1.1. Effect of adsorption time

The impact of contact time on the efficiency and adsorption capacity of Cu^{2+} by halloysite over time is illustrated in Fig. 3a. The results

Table 1
CV scanning parameters for 0.005 M Cu^{2+} and 1 g Cu-HAL in reline.

Parameter	Value	Parameter	Value
WE	Au (S = 0.0201 cm^2)	Potential step	0.005 V
RE	$Ag/AgCl/Cl^-$	Scanning rate	0.02 V/S
CE	Pt	V_{reline}	5 mL
Potential range	0.1 V ÷ − 0.9 (V)	-	-

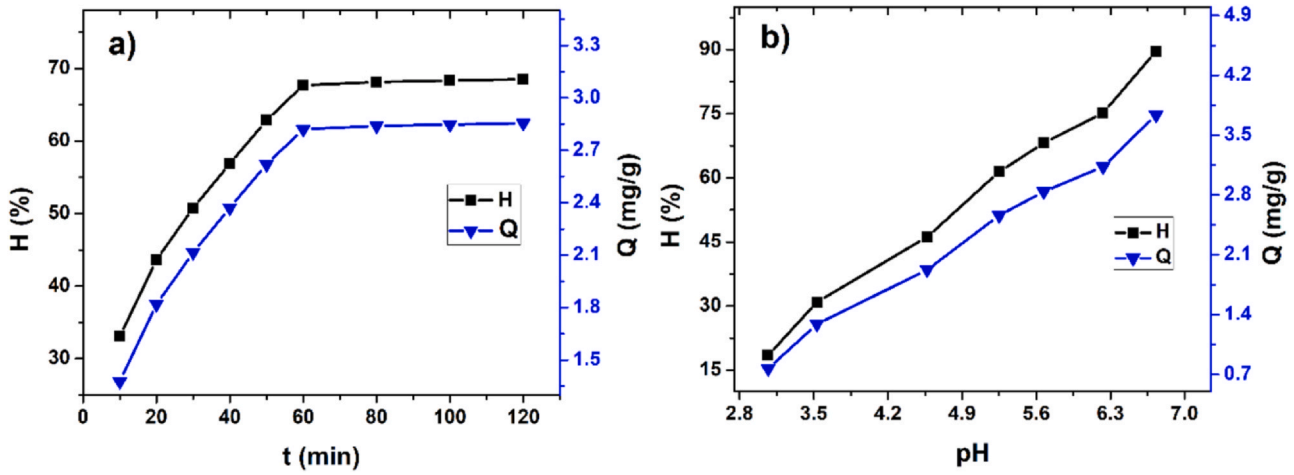

Fig. 3. The effect of contact time at a $C_{Cu^{2+}}$ = 50 mg/L, m_{HAL} = 0.6 g, T = 25°C, pH = 5.3 and pH at a $C_{Cu^{2+}}$ = 50 mg/L, m_{HAL} = 0.6 g, T = 25°C, t = 80 min (b) on the halloysite's adsorption of Cu^{2+}.

indicate that as the contact time increases, both the adsorption capacity and efficiency also increase. Within the studied period, ranging from 10 min to 120 min, the adsorption capacity experiences a rapid increase during the first 60 min, followed by a slower increase from 60 to 80 min. After 80 min, the efficiency and adsorption capacity stabilize at approximately 68% and 2.8 mg/g, respectively. As a result, a contact time of 80 min was selected for the Cu^{2+} adsorption process in subsequent studies.

3.1.2. Effect of pH

The removal of Cu^{2+} ions is significantly dependent on the pH of the solution because pH has a pronounced effect on the surface properties of the adsorbent and existent species of metal ions in the solution [42]. To prevent the formation of $Cu(OH)_2$ precipitate in an alkaline environment, the influence of pH was studied under conditions where pH $\leq$ 7 and around the pH_{PZC} value (zero charge point). The variation in adsorption capacity and efficiency with pH is depicted in Fig. 3b. Notably, within the tested pH range, both efficiency and adsorption capacity increase with rising pH. This result can be attributed to the protonation of halloysite in acidic environments, which causes the surface of the particles to become positively charged [43]. This, in turn, reduces the number of available adsorption sites on halloysite and leads to competitive adsorption between H^+ ions and Cu^{2+} ions, consequently diminishing adsorption capacity. As pH increases, the positive charge density on the surface decreases, enhancing the ability to adsorb Cu^{2+} ions until reaching a pH higher than pH_{PZC}, which is favorable for Cu^{2+} ion adsorption. Hence, a pH value of 6.2 was chosen for the Cu^{2+} ion adsorption process in subsequent studies.

3.1.3. Effect of halloysite mass

The adsorption process was conducted using varying amounts of halloysite, ranging from 0.3 g to 1.0 g (see Fig. 4a). The research results indicate that as the mass of halloysite increases from 0.3 g to 0.6 g, the adsorption capacity decreases from 3.42 to 3.13 mg/g, meanwhile the efficiency rapidly increases from 41.04% to 75.8% due to the increase of contact area between the adsorbent and the solution, so there are more active centers for adsorption [43]. Within the range of changing the mass of the adsorbent material from 0.6 g to 1 g, the adsorption efficiency increases at a slower rate. However, when the amount of adsorbent material continues to increase, the efficiency remains nearly unchanged as adsorption reaches equilibrium, while the adsorption capacity decreases. To strike a suitable balance between adsorption capacity and efficiency (2.55 mg/g; 81.66%), we selected a mass of 0.8 g of halloysite for the study of Cu^{2+} ion adsorption.

3.1.4. Effect of initial Cu^{2+} concentration

The initial concentration of Cu^{2+} significantly affects both the adsorption capacity and efficiency. Results from the investigation of the adsorption process, using a range of initial Cu^{2+} concentrations from 10 mg/L to 80 mg/L, demonstrate that as the Cu^{2+} concentration

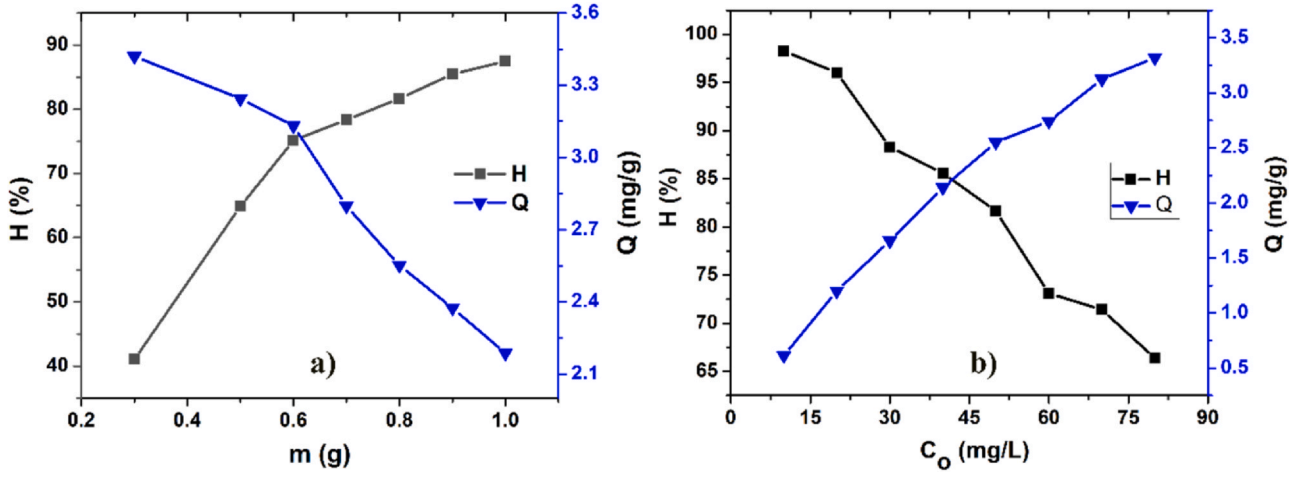

Fig. 4. The effect of halloysite mass at $C_{Cu^{2+}}$ = 50 mg/L, T = 25°C, pH = 6.2, and t = 80 min (a) and initial Cu^{2+} concentration m_{HAL} = 0.8 g, pH = 6.2, T = 25 °C, t = 80 mins (b) on the halloysite's adsorption of Cu^{2+}.

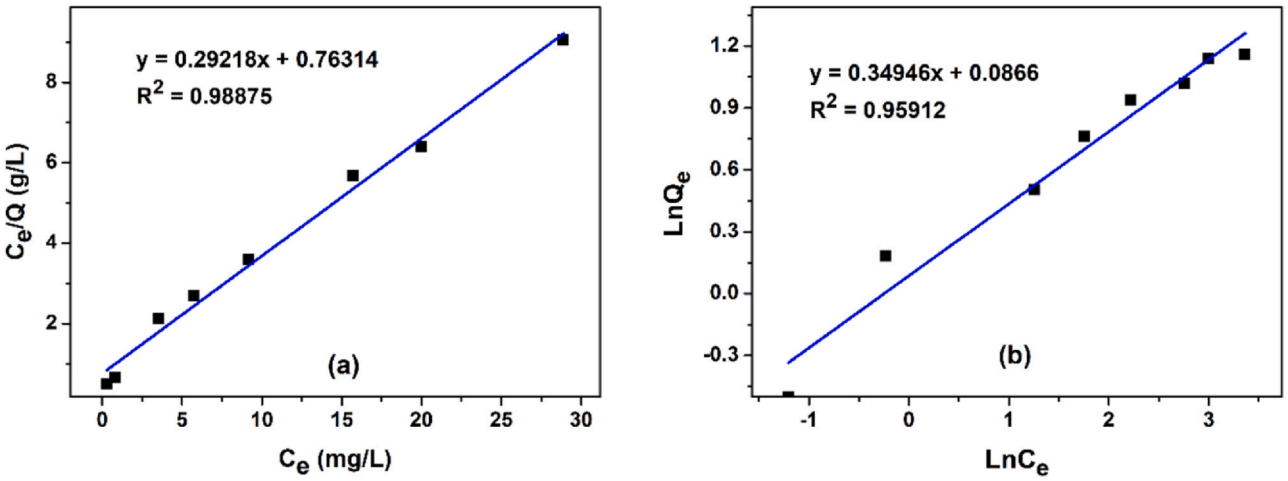

Fig. 5. Cu^{2+} adsorption isotherm at 25 °C according to Langmuir (a) and Freundlich (b).

increases, the adsorption capacity gradually rises, while the adsorption efficiency decreases (Fig. 4b). This was explained by the solution concentration increases, the amount of Cu^{2+} ions increases, but the adsorption capacity of halloysite is gradually saturated, so the adsorption efficiency will decrease [44]. To simultaneously achieve high adsorption capacity and efficiency, an appropriate Cu^{2+} concentration within the range of 30 to 50 mg/L is selected. At a Cu^{2+} concentration of 40 mg/L, the adsorption capacity and efficiency reach 2.14 mg/g and 85.19%, respectively. This result indicates the higher adsorption efficiency of halloysite for Cu^{2+} comparable to other investigated heavy metal ions, such as Cd^{2+} - 51.45% and Pb^{2+} - 79.3% [45], as well as As (III) - 82.4% [44]. However, the adsorption capacity is lower than the modified halloysite [8].

3.2. Adsorption isotherm

The Cu^{2+} adsorption experiments were carried out under the following conditions: 0.8 g of halloysite was placed in a 50 mL solution of Cu^{2+} with varying initial concentrations. The mixtures were exposed for 80 min at a pH of 6.2 and room temperature (25 °C). Afterward, the remaining Cu^{2+} concentration at equilibrium (C_e) was determined. This data enabled the calculation of values such as lnC_e, lnQ, the C_e/Q ratio, and the construction of Langmuir (see Fig. 5a) and Freundlich (Fig. 5b) isotherm equations.

From the isotherm plots, we can determine experimental parameters such as the maximum adsorption capacity according to the Langmuir isotherm (Q_m), the Langmuir constant (K_L), and the experimental parameters for the Freundlich isotherm (K_F, n). The results, as summarized in Table 2, clearly indicate that the adsorption of Cu^{2+} on the halloysite conforms to the Langmuir adsorption model. This result also fits with the last reports using halloysite and halloysite-based adsorbents for adsorption of heavy metal ions [8,10].

3.3. Adsorption kinetics

Based on the results obtained from the study on the influence of adsorption time on Cu^{2+} adsorption capacity, graphs depicting the pseudo-first-order (according to Eq. 6) and pseudo-second-order (according to Eq. 7) kinetic adsorption equations have been constructed, as illustrated in Fig. 6.

From the graphs presented in Fig. 6, we calculated the rate constants (k) and equilibrium adsorption capacities (Q_e), and the results are summarized in Table 3. The Q_e value calculated using the pseudo-first-order kinetic adsorption equation (4.182 mg/g) notably deviates from the experimental Q_e value (2.854 mg/g). In contrast, the Q_e value calculated using the pseudo-second-order kinetic adsorption equation (3.251 mg/g) is much closer to the experimental value. Moreover, the regression coefficient (R^2) for the pseudo-second-order kinetic equation is nearly 1 (R^2 = 0.99502), indicating a strong fit, while the R^2 value for the pseudo-first-order kinetic equation (0.94374) is considerably lower. These results strongly suggest that the adsorption of Cu^{2+} by halloysite follows the pseudo-second-order kinetic adsorption equation, which is consistent with many earlier other literature [8,10]. The determined rate constant for adsorption has a value of 0.0223 g/mg/min.

Table 2
Experimental constants Q_m, K_L, K_F, n in the Langmuir and Freundlich equations of Cu^{2+} adsorption process.

Langmuir			Freundlich		
Q_m	K_L	R^2	N	K_F	R^2
3.42	0.38315	0.98875	2.8615	1.09046	0.95912

3.4. Characterization of HAL before and after the adsorption process

The characterizations of HAL powder before and after the adsorption process were analyzed using FT-IR, XRD, and SEM-EDX. The FT-IR spectra revealed that the Cu^{2+} adsorption process did not alter the functional groups within the HAL molecule (see Fig. 7a). XRD patterns of HAL were found to be like those of the Cu-HAL sample with peaks representing the minerals HAL and kaolinite (see Fig. 7b). SEM images of HAL before and after Cu^{2+} adsorption are presented in Fig. 8, showcasing a nanotubular morphology for both. Notably, the particle size and shape remained largely unchanged after the Cu^{2+} adsorption process. The EDX spectra confirmed the presence of copper in HAL following the adsorption process.

3.5. Desorption of Cu^{2+} and recovery of Cu metal

3.5.1. Cyclic voltammograms of $Cu(NO_3)_2$ and Cu-HAL in reline electrolyte

The results presented in Fig. 12 indicate the presence of a reduction peak of Cu^{2+} at − 0.6 V and an oxidation peak of Cu^0 at − 0.4 V in the cyclic voltammetry curves of reline, which contain not only $Cu(NO_3)_2$ (Fig. 9a) but also Cu-HAL (Fig. 9b). This observation aligns with previous reports on the cyclic voltammetry of Cu^{2+} in reline [46–48]. Furthermore, Fig. 9b demonstrates the presence of a reduction peak of Cu^{2+} at − 0.6 V and an oxidation peak of Cu^0 at − 0.4 V in the cyclic voltammetry curve of reline containing $Cu(NO_3)_2$, similar to the behavior observed in Cu-HAL. The mechanism of the deposition and dissolution of Cu on the Au electrode can be described as follows [49–51]:

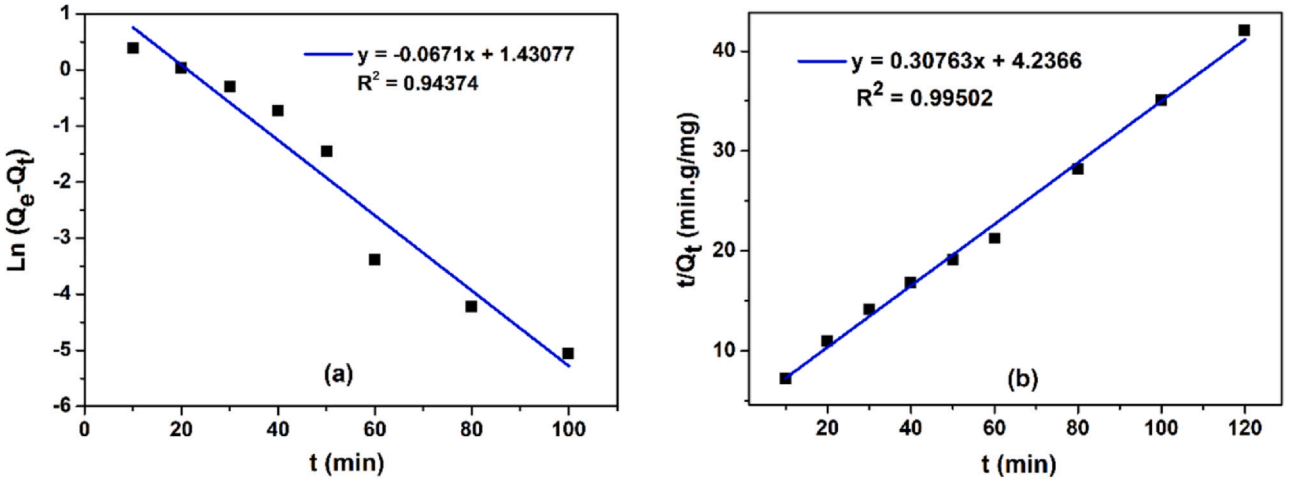

Fig. 6. Isotherm plots for the adsorption of Cu^{2+} onto halloysite according to pseudo-first-order kinetic equation (a) and pseudo-second-order kinetic equation (b).

Table 3
Values of k and Q_e calculated by pseudo-first-order and pseudo-second-order kinetic equations.

pseudo-first-order kinetic model			pseudo-second-order kinetic model			Q_e experiment ($mg.g^{-1}$)
Q_e ($mg.g^{-1}$)	k_1 (min^{-1})	R^2	Q_e ($mg.g^{-1}$)	k_2 (g/mg/min)	R^2	
4.182	0.0671	0.94374	3.251	0.0223	0.99502	2.854

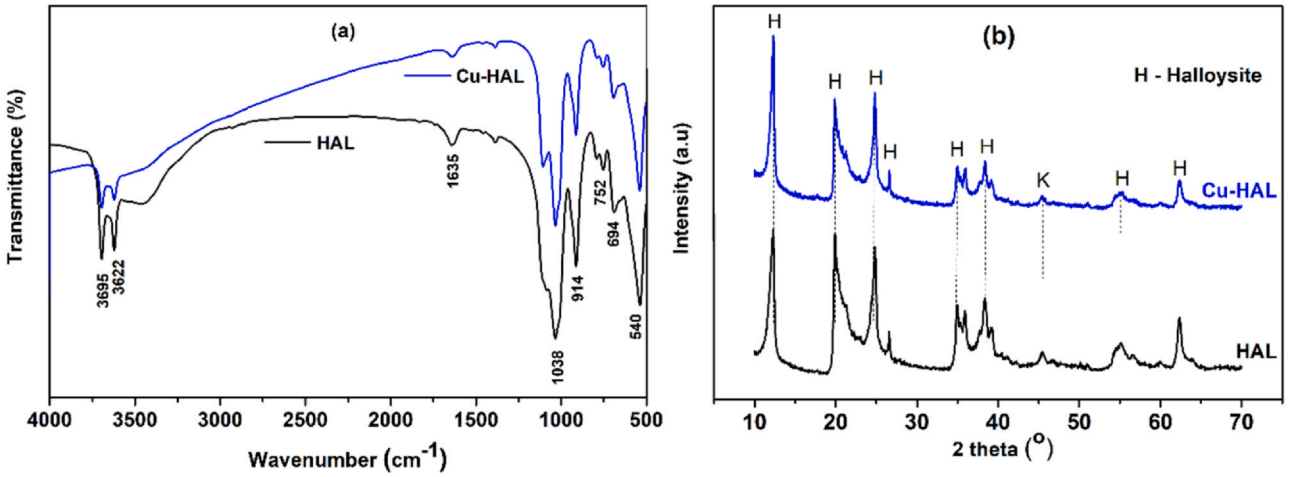

Fig. 7. FT-IR spectra (a) and XRD patterns (b) of HAL before and after Cu^{2+} adsorption process.

Step 1: Formation of a complex between Cu^{2+} from Cu-HAL and Cl^- from reline, resulting in $CuCl_n^{2-n}$. Subsequently, the reduction of Cu^{2+} (in $CuCl_n^{2-n}$) to Cu metal occurs on the surface of the electrode: $CuCl_n^{2-n} + 2e \rightarrow Cu + nCl^-$.

Step 2: Stripping of Cu metal to Cu^{2+}: $Cu - 2e \rightarrow Cu^{2+}$.

The cyclic voltammetry results for Cu-HAL in the reline solvent demonstrate that Cu^{2+} ions can be desorbed from the loaded HAL material and subsequently reduced to Cu metal on the surface of an Au electrode in reline solvent, allowing for the recovery and reuse of the HAL adsorbent. The deposition of Cu metal onto the Au electrode surface can be achieved at potentials ≤ -0.6 V.

3.5.2. Effect of several impacts on the ability of desorption and copper recovery

Cu^{2+} ions were successfully desorbed from Cu-HAL, and Cu metal was efficiently recovered through the electrodeposition method into a reline solvent, utilizing applied current techniques. The deposition of Cu on the surface of the Au electrode is visually depicted in Fig. 10.

3.5.2.1. Influence of applied current. Cathodic polarization curves of the Au electrode were generated at various applied current values for 2 h at a temperature of 60 °C. The recovery efficiency of Cu is presented in Table 4.

It was observed that Cu^{2+} ions were desorbed from the loaded HAL material, and Cu metal was deposited on the surface of the Au plate electrode. The electrodeposition of Cu metal was dependent on the applied current. As the applied current increased, the amount of Cu deposited on the surface of the Au electrode also increased, resulting in higher Cu recovery efficiency (as shown in Table 4). After 2 h of electrolysis at an applied current of 10 mA, the Cu recovery efficiency reached 73.61%. However, to avoid excessive current, which could lead to sub-processes and maintain a reasonably high Cu recovery efficiency, we selected an applied current of 7.5 mA for subsequent studies.

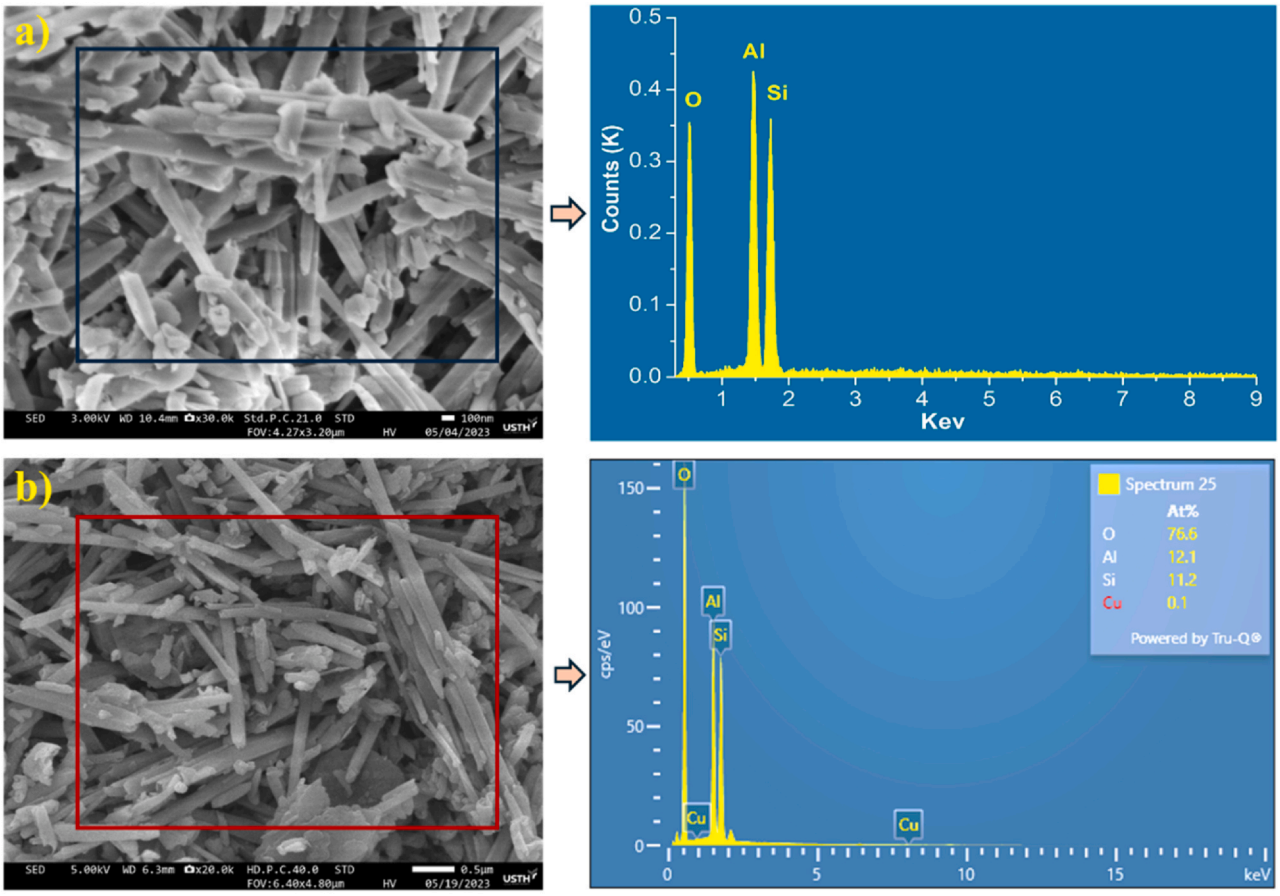

Fig. 8. SEM-EDX analysis of HAL (a) and Cu-HAL (b).

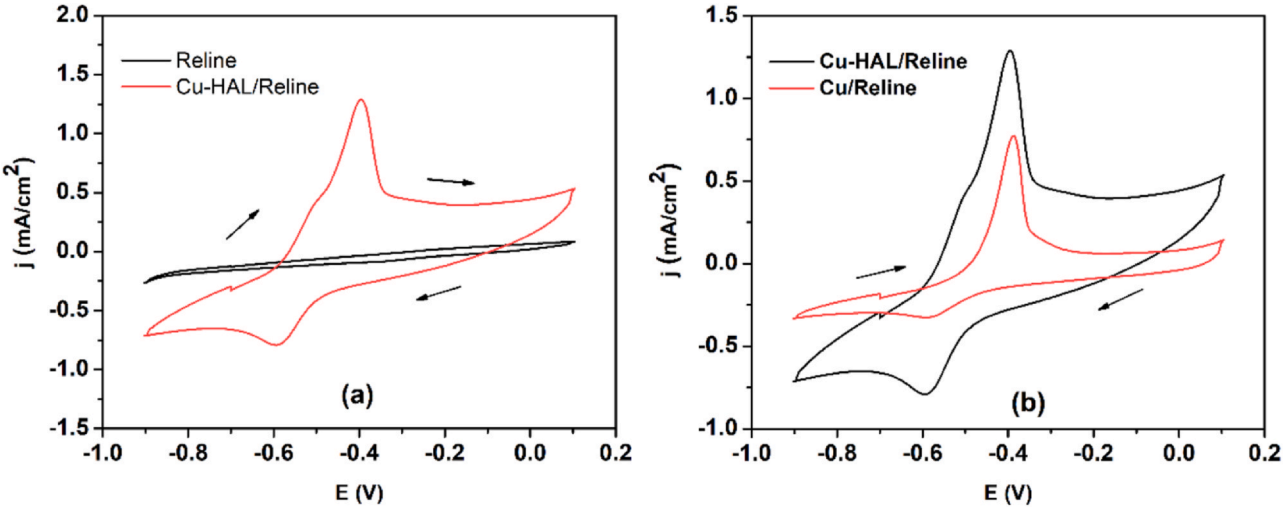

Fig. 9. CVs of $Cu(NO_3)$ (a) and Cu-HAL (b) in the electrolyte of reline.

3.5.2.2. Influence of Cu-HAL mass. The recovery efficiency of Cu was found to be dependent on the mass of Cu-HAL. Increasing the mass of Cu-HAL resulted in a higher amount of Cu deposited on the surface of the Au electrode, but it also led to a decrease in Cu recovery efficiency due to the time is not enough to release an amount of Cu^{2+} completely from the adsorption material, as shown in Table 5. The highest Cu recovery efficiency, reaching 82.68%, was achieved with a mass of 0.3 g Cu-HAL. Therefore, 0.3 g of Cu-HAL was selected for further investigation.

3.5.2.3. Influence of electrolytic time. Table 6 illustrates the variation in Cu recovery efficiency concerning electrolysis time. As electrolysis time

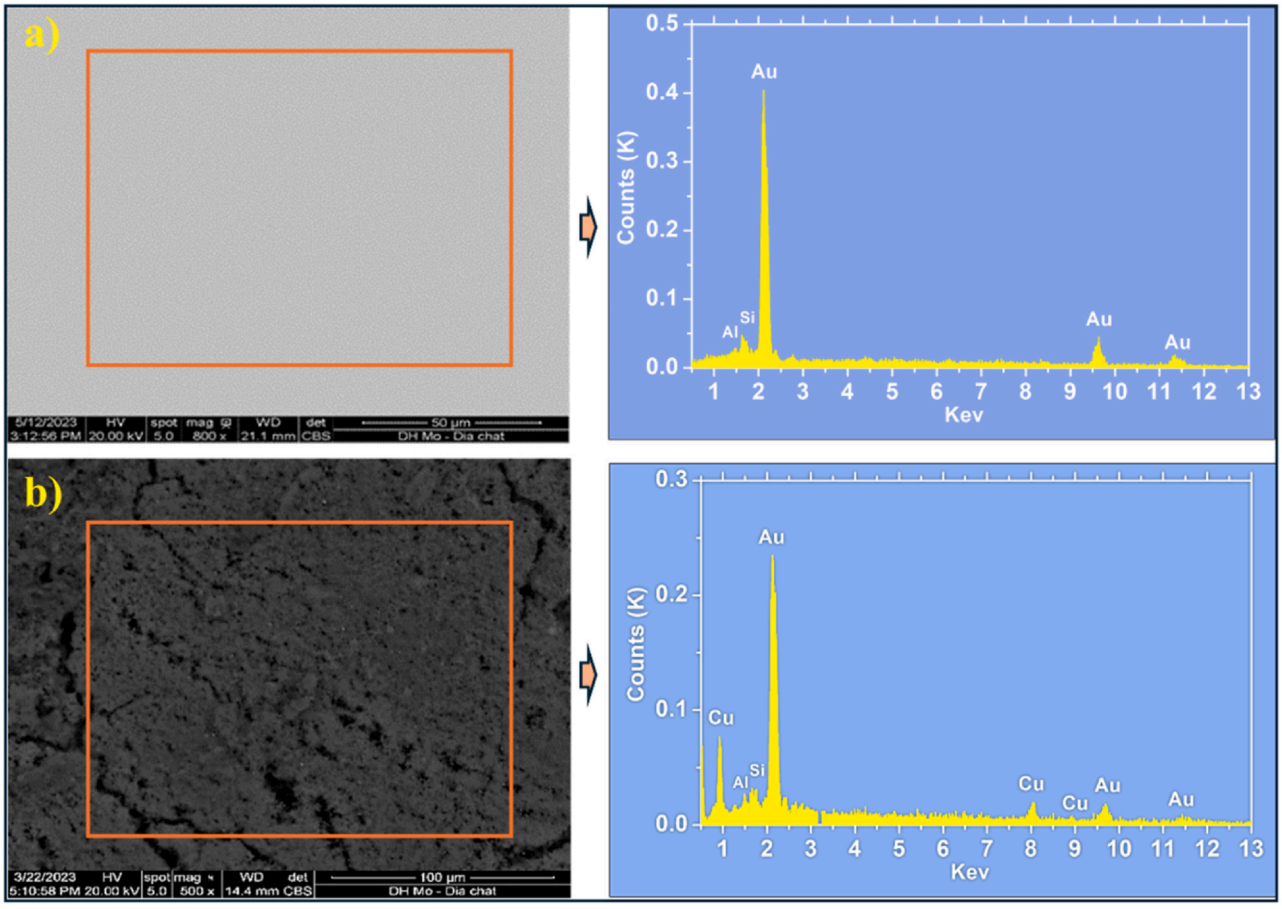

Fig. 10. SEM-EDX analysis of the surface of Au electrode after electrolysis Cu-HAL.

Table 4
The recovery efficiency of Cu (H %) from 0.5 g Cu-HAL at different apply currents for 2 h.

Current (mA)	0.5	1	2	3	5	7.5	10
Recovery efficiency (%)	42.50	45.68	47.42	52.11	60.48	69.72	73.61

Table 5
The recovery efficiency of Cu with different Cu-HAL masses at 7.5 mA applied current for 2 h.

Cu-HAL mass (g)	0.3	0.5	0.7	1.0
Recovery efficiency (%)	82.68	69.72	58.8	51.36

increases, the amount of Cu deposited on the surface of the Au electrode also rises, increasing Cu recovery efficiency. The recovery efficiency of Cu shows a gradual increase as the electrolytic time changes from 1 to 7 h, and it increases at a slower rate after 7 h. At an electrolytic time of 10 h, the recovery efficiency of Cu reaches 98.26%, which is only a slight improvement compared to the 97.52% achieved at 7 h. To achieve a high recovery efficiency of Cu (97.52%) without an excessively long electrolysis time, 7 h was selected for the electrolysis and recovery of Cu.

3.6. Regeneration of material after the desorption

During the electrolysis process, Cu^{2+} ions were successfully desorbed from the loaded HAL material, allowing for the recovery of HAL material for further adsorption. As shown in Fig. 11, the SEM image of the obtained HAL after electrolysis closely resembled the initial HAL material, retaining its tubular structure. Additionally, the EDX spectra indicated peaks characteristic of HAL, with no discernible Cu peaks. FT-IR spectra of the initial HAL and reused HAL showed no significant differences (see Fig. 12), indicating that the HAL material remained unaltered after the electrolysis. This suggests that Cu^{2+} ions were effectively released from Cu-HAL, and the HAL material remained unmodified. To assess the regeneration potential of the HAL sorbent, adsorption experiments were conducted under suitable conditions for Cu^{2+} adsorption. The results demonstrated that the adsorption capacity and efficiency could reach 2.15 mg/g and 86.20%, respectively, after

Table 6
The recovery efficiency of Cu at different time.

Electrolysis time (h)	1	2	3	4	5	7	10
Recovery efficiency (%)	75.79	82.68	87.79	91.41	94.65	97.52	98.26

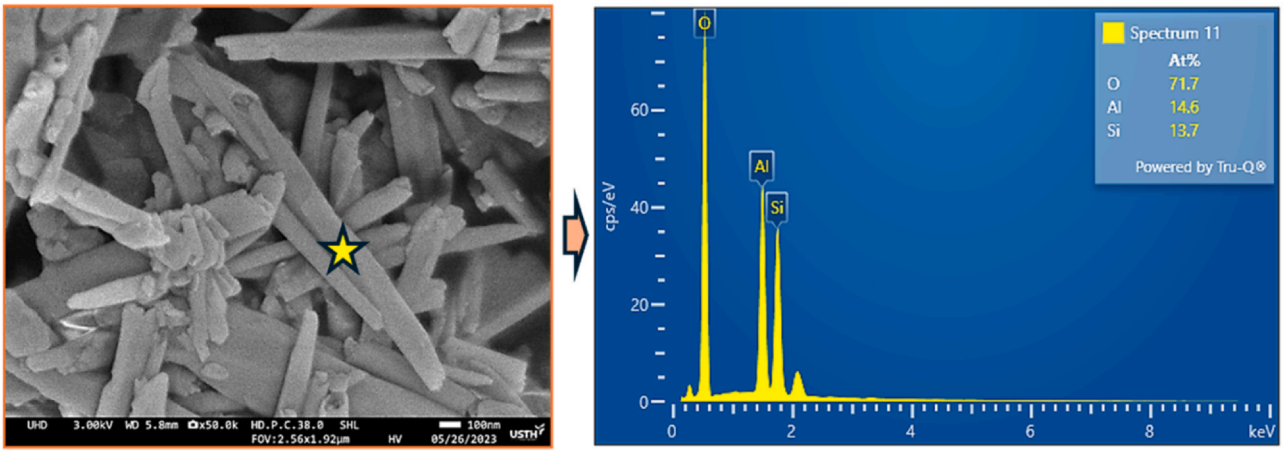

Fig. 11. SEM-EDX analysis of the HAL material after the desorption.

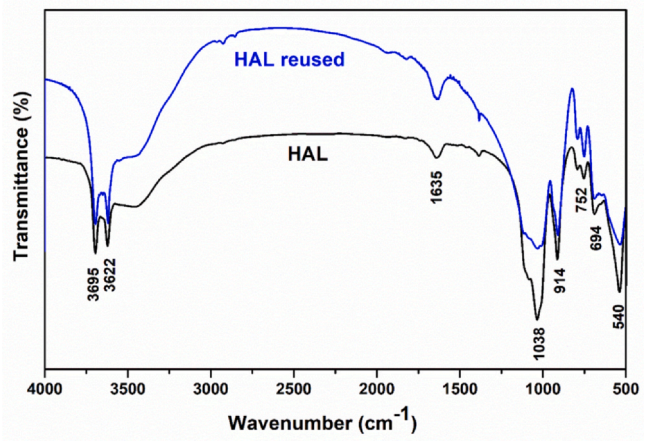

Fig. 12. FT-IR spectra of the initial and after the desorption/reused HAL material.

the first adsorption-desorption cycle; 2.12 mg/g and 84.67% after the second cycle; and 2.10 mg/g and 84.52% after the third cycle. These findings illustrate that the regenerated HAL material exhibits significant adsorption capacity and efficiency for Cu^{2+} ions.

4. Conclusions

Halloysite clay minerals have been employed for an integrated process that encompasses the adsorption of Cu^{2+} ions, subsequent desorption, Cu metal recovery, and the regeneration of adsorbent materials. The findings indicate that the adsorption process is subject to various influencing factors, including pH, initial Cu^{2+} concentration, adsorbent mass, and contact time. Consequently, specific conditions were chosen for treating Cu^{2+} in water: a halloysite mass of 0.6 g per 50 mL of solution, an initial Cu^{2+} concentration ranging from 30 to 50 mg/L, an 80-minute contact time, pH 6.2, and room temperature (25 °C). The adsorption process adheres to the Langmuir isotherm model, displaying a maximum adsorption capacity of 3.42 mg/g, and follows second-order pseudo kinetics. Under the studied adsorption conditions with an initial Cu^{2+} concentration of 40 mg/L, the adsorption capacity and efficiency reached 2.14 mg/g and 85.19%, respectively. Importantly, the desorption of Cu^{2+} from the HAL material and the recovery of Cu metal were conducted simultaneously, obviating the need for a pre-desorption step, in a DES solution using the electrochemical precipitation method. This represents a significant advantage and novelty in this publication. The results demonstrate that 97.52% of the Cu metal content can be recovered after 7 h of electrolysis with a current density of 7.5 mA at 60 °C. Following the Cu metal separation process, the HAL material can be reused for subsequent adsorption processes, achieving an adsorption capacity and efficiency about of 2.1 mg/g and > 84.5% after three cycles of adsorption-desorption under the studied suitable conditions. This outcome opens the potential for utilizing halloysite clay minerals to remove Cu^{2+} ions from polluted water and recover Cu metal directly from loaded material without elute solvent, avoid secondary pollution and recover useful metals from waste sources.

Declaration of Competing Interest

The authors declare that they have no known competing financial interests or personal relationships that could have appeared to influence the work reported in this paper.

Acknowledgements

Thank you to the project of the Ministry of Education and Training of Vietnam, the code number B2022-MDA-03, for helping complete this research.

References

[1] Bai B, Bai F, Li X, Nie Q, Jia X, Wu H. The emediation efficiency of heavy metal pollutants in water by industrial red mud particle waste. Environ Technol Innov 2022;28:102944.
[2] Kuldeyev E, Seitzhanova M, Tanirbergenova S, Tazhu K, Doszhanov E, Mansurov Z, Azat S, Nurlybaev R, Berndtsson R. Modifying natural zeolites to improve heavy metal adsorption. Water 2023;15(12):2215.
[3] Hieu DTM, Thao TPT, Khoa TA, Vien LM. A novel method for the fabrication of granular hydroxyapatite-bentonite composite adsorbents for the removal of Pb^{2+} from an aqueous solution. J Environ Sci Eng B 2016;5:371–8.
[4] Quaghebeur M, Rengel Z, Rate AW, Hinz C. Heavy metals in the environment desorption kinetics of arsenate from kaolinite as influenced by pH. J Environ Qual 2005;34:479–86.
[5] Aliabadi M, Irani M, Ismaeili J, Najafzadeh S. Design and evaluation of chitosan/hydroxyapatite composite nanofiber membrane for the removal of heavy metal ions from aqueous solution. J Taiwan Inst Chem Eng 2013. https://doi.org/10.1016/j.jtice.2013.04.016.
[6] Shanika FM, de Silva RM, de Silva NKM. Synthesis, characterization, and application of nano hydroxyapatite and nanocomposite of hydroxyapatite with granular activated carbon for the removal of Pb^{2+} from aqueous solutions. Appl Surf Sci 2015;351:95–103.
[7] Bahdod A, El Asri S, Saoiabi A, Coradin T, Laghzizil A. Adsorption of phenol from an aqueous solution by selected apatite adsorbents: Kinetic process and impact of the surface properties. Water Res 2009;43:313–8.
[8] Anastopoulos I, Mittal A, Usman M, Mittal J, Yu G, Núñez-Delgado A, Kornaros M. A review on halloysite-based adsorbents to remove pollutants in water and wastewater. J Mol Liq 2018;269:855–68. https://doi.org/10.1016/j.molliq.2018.08.104.
[9] Danyliuk N, Tomaszewska J, Tatarchuk T. Halloysite nanotubes and halloysite-based composites for environmental and biomedical applications. J Mol Liq 2020;309:113077. https://doi.org/10.1016/j.molliq.2020.113077.
[10] Maziarz P, Matusik J. The effect of acid activation and calcination of halloysite on the efficiency and selectivity of Pb(II), Cd(II), Cu(II) and As(V) uptake. Clay Min 2016;51:385–94.

[11] Muniyappan RG, Kousalya GN, Meenakshi S. Removal of copper(II) using chitin/chitosan nano-hydroxyapatite composite. Int J Biol Macromol 2011;48:119–24.
[12] Hamzaoui M, Bestani B, Benderdouche N. The use of linear and nonlinear methods for adsorption isotherm optimization of basic green 4-dye onto sawdust-based activated carbon. J Mater Environ Sci 2018;9(4):1110–8.
[13] Khanday WA, Asif M, Hameed BH. Cross-linked beads of activated oil palm ash zeolite/chitosan composite as a bio-adsorbent for the removal of methylene blue and acid blue 29 dyes. Int J Biol Macromol 2016. https://doi.org/10.1016/j.ijbiomac.2016.10.075.
[14] Arbabi M, Hemati S, Shamsizadeh Z, Arbabi A. Nitrate removal from aqueous solution by almond shells activated with magnetic nanoparticles. Desalin Water Treat 2017;80:344–51.
[15] Marrakchi F, Ahmed MJ, Khanday WA, Asif M, Hameed BH. Mesoporous-activated carbon prepared from chitosan flakes via single-step sodium hydroxide activation for the adsorption of methylene blue. Int J Biol Macromol 2017;98:233–9.
[16] Azharul Islam Md, Ahmed MJ, Khanday WA, Asif M, Hameed BH. Mesoporous activated carbon prepared from NaOH activation of rattan (Lacosperma secundiflorum) hydrochar for methylene blue removal. Ecotoxicol Environ Saf 2017;138:279–85.
[17] Yuan P, Tan D, Annabi-Bergaya F. Properties and applications of halloysite nanotubes: Recent research advances and future prospects. Appl Clay Sci 2015;112-113:75–93.
[18] Zhang Y, Tang A, Yang H, Ouyang J. Applications and interfaces of halloysite nanocomposites. Appl Clay Sci 2016;119:8–17.
[19] Danyliuk N, Tomaszewska J, Tatarchuk T. Halloysite nanotubes and halloysite-based composites for environmental and biomedical applications. J Mol Liq 2020;309:113077.
[20] Parisi F, Lazzara G, Merli M, Milioto S, Princivalle F, Sciascia L. Simultaneous Removal and Recovery of Metal Ions and Dyes from Wastewater through Montmorillonite Clay Mineral. Nanomaterials 2019;9:1699. https://doi.org/10.3390/nano9121699.
[21] Kurczewska J, Cegłowski M, Schroeder G. Alginate/PAMAM dendrimer - Halloysite beads for removal of cationic and anionic dyes. Int J Biol Macromol 2019;123:398–408.
[22] Maziarza P, Matusika J, Radziszewska A. Halloysite-zero-valent iron nanocomposites for removal of Pb(II)/Cd(II) and As(V)/Cr(VI): Competitive effects, regeneration possibilities and mechanisms. J Environ Chem Eng 2019;7(6):103507.
[23] Pirhaji JZ, Moeinpour F, Dehabadi AM, Ardakani SAY. Synthesis and characterization of halloysite/graphene quantum dots magnetic nanocomposite as a new adsorbent for Pb(II) removal from water. J Mol Liq 2020;300:112345.
[24] Ramanayaka S, Sarkar B, Coorayc AT, Oke YS, Vithanage M. Halloysite nanoclay supported adsorptive removal of oxytetracycline antibiotic from aqueous media. J Hazard Mater 2020;384:121301.
[25] Sheha RR. Sorption behaviour of Cu(II) ions on synthesized hydroxyapatite. J Colloid Interface Sci 2007;310(1):18–26.
[26] ITAMI K, YANAI J. Sorption and desorption properties of Cadmium and Copper on soil clays in relation to charge characteristics. Soil Sci Plant Nutr 2006;52:5–12.
[27] Lukman S, Essa M, Mu`azu N, Bukhari A, Basheer C. Adsorption and Desorption of Heavy Metals onto Natural Clay Material: Influence of Initial pH. J Environ Sci Technol 2013;6(1):1–15.
[28] Peld M, Tonsuaadu K, Bender V. Sorption and desorption of Cd^{2+} and Zn^{2+} ions in apatite-aqueous systems. Environ Sci Technol 2004;38:5626–31.
[29] Chen J, Wang Y, Zhou D, Cui Y, Wang S, Chen Y. Adsorption and Desorption of Cu (II), Zn(II), Pb(II), and Cd(II) on the Soils amended with nanoscale hydroxyapatite. Environ Prog Sustain Energy 2010;29(2):233–41.
[30] Chand P, Pakade YB. Synthesis and characterization of hydroxyapatite nanoparticles impregnated on apple pomace to enhanced adsorption of Pb(II), Cd(II), and Ni(II) ions from aqueous solution. Environ Sci Pollut Res 2015;22:10919–29.
[31] Xie S, Wen Z, Zhan H, Jin M. An experimental study on the adsorption and desorption of Cu(II) in silty clay, Hindawi (Volume). Geofluids2018:12.
[32] Rehman S, Huang Z, Wu P, Ahmed Z, Ye Q, Liu J, Zhu N. Adsorption of lead and antimony in the presence and absence of EDTA by a new vermiculite product with potential recyclability. Environ Sci Pollut Res 2021;28(35):49112–24.
[33] Cela-Dablanca R, Barreiro A, Ferreira-Coelho G, Campillo-Cora C, Pérez-Rodríguez P, Arias-Estévez M, Núñez-Delgado A, Álvarez-Rodríguez E, Fernández-Sanjurjo MJ. Cu and As(V) Adsorption and Desorption on/from Different Soils and Bio-Adsorbents. Materials 2022;15(14):5023.
[34] J. Feng, J. Shi, Effect of nanoscale hydroxyapatite on soil adsorption and desorption of heavy metals, November 2015, ⟨doi:10.3785/j.issn.1008–9497.2015.06.017⟩.
[35] Jurgelane I, Locs J. Activated carbon and clay pellets coated with hydroxyapatite for heavy metal removal: characterization. Adsorpt, Regen, Mater 2023;16(9):3605.
[36] Patel PK, Pandey LM, Uppaluri R. Multi-metal adsorption and cyclic desorption characteristics of Zn^{+2} and Cu^{+2} constituting multi-component synthetic wastewater system using commercial resins. Sustain Environ 2023:3–27.
[37] Pan H, Zhao X, Zhou X, Yan H, Han X. Research progress on the role of biofilm in heavy metals adsorption-desorption characteristics of microplastics: A review. Environ Pollut 2023;336:122448.
[38] Zhang C, Yuan Y, Li T. Adsorption and desorption of heavy metals from water using aminoethyl reduced graphene oxide. Environ Eng Sci 2018;35(9). https://doi.org/10.1089/ees.2017.0541.
[39] Mishra S. Adsorption-desorption of heavy metal ions. Curr Sci 2014;107(4):601–12.
[40] Smičiklas I, Onjia A, Raičević S. Experimental design approach in the synthesis of hydroxyapatite by neutralization method. Sep Purif Technol 2005;44:97–102.
[41] Rayée Q, Doneux T, Buess-Herman C. Underpotential deposition of silver on gold from deep eutectic electrolytes. Electrochim Acta 2017;237:127–32.
[42] Abdel-Fadeel MA, Aljohani NS, Al-Mhyawi SR, Halawani RF, Aljuhani EH, Salam MA. A simple method for removal of toxic dyes such as Brilliant Green and Acid Red from the aquatic environment using Halloysite nanoclay. J Saudi Chem Soc 2022;26:101475.
[43] Dou W, Deng Z, Fan J, Lin Q, Wu Y, Ma Y, Li Z. Enhanced adsorption performance of La(III) and Y(III) on kaolinite by oxalic acid intercalation expansion method. Appl Clay Sci 2022;229:106693.
[44] Aljohani NS, Kavil YN, Al-Farawati RK, Alelyani SS, Orif MI, Shaban YA, Al-Mhyawi SR, Aljuhani EHX, Salam MA. The effective adsorption of arsenic from polluted water using modified Halloysite nanoclay. Arab J Chem 2023;16:104652.
[45] Bui HB, Nguyen H, Nguyen TTT, Le TD, Vo TH, Nguyen TD, Luong QK, Do MA. Performance evaluation of nanotubular halloysites from weathered pegmatites in removing heavy metals from water through novel artificial intelligence-based models and human-based optimization algorithm. Chemosphere 2021;282:131012.
[46] Sebastián P, Torralba E, Vallés E, Molina A, Gómez E. Advances in Copper Electrodeposition in Chloride Excess. A Theoretical and Experimental Approach. Electrochim Acta 2015;164:187–95.
[47] Sebastián P, Gómez E, Climent V, Feliu JM. Copper underpotential deposition at gold surfaces in contact with a deep eutectic solvent: New insights. Electrochem Commun 2017;78:51–5.
[48] Spathariotis S. Recovery of metals using deep eutectic solvents (Thesis). University of Leicester,; January 2020.
[49] Abbott AP, Ballantyne A, Harris RC, Juma JA, Ryder KS, Forrest G. A Comparative Study of Nickel Electrodeposition Using Deep Eutectic Solvents and Aqueous Solutions. Electrochim Acta 2015;176:718–26.
[50] Starykevich M, Salak AN, Ivanou DK, Lisenkov AD, Zheludkevich ML, Ferreira MGS. Electrochemical deposition of zinc from deep eutectic solvent on barrier alumina layers. Electrochim Acta 2015;170:284–91.
[51] Shishov A, Bulatov A, Locatelli M, Carradori S, Andruch V. Application of deep eutectic solvents in analytical chemistry. A review. Microchem J 2017;135:33–8.